Electronic Research Archive

https://www.aimspress.com/journal/era

ERA, 34(9): 6219–6248.
DOI: 10.3934/era.2026273
Received: 11 May 2026
Revised: 04 July 2026
Accepted: 06 July 2026
Published: 16 July 2026

Research article

Dynamics of a stage-structured amensalism model with fear effect: stability and transcritical bifurcation analysis

Xiaoran Li[1,2], Qin Yue[1,*] and Fengde Chen[3,*]

[1] School of Finance and Mathematics, West Anhui University, Lu'an 237000, China
[2] Faculty of Economics and Business, Universiti Malaysia Sarawak, Kota Samarahan, Malaysia
[3] School of Mathematics and Statistics, Fuzhou University, Fuzhou 350108, China

* **Correspondence:** Email: zzj901010@163.com, fdchen@fzu.edu.cn.

Abstract: This paper studies a stage-structured two-species amensalism model incorporating fear effects on the inhibited species. Extending the framework of Lei, we introduce a single fear parameter f that simultaneously suppresses adult reproduction and amplifies adult mortality via a saturating Holling-Type II response, ensuring that the total adult mortality rate under fear remains biologically bounded by $2\delta_2$. We establish a threshold-based dynamic classification in the biologically feasible region governed by a net reproduction number $\mathcal{N}_0$ and a critical threshold f_{crit}. When $\mathcal{N}_0 > 1$ and $0 \le f < f_{\text{crit}}$, the coexistence equilibrium is globally asymptotically stable, which can be proved via a Volterra-type logarithmic Lyapunov function; when $f \ge f_{\text{crit}}$, the extinction equilibrium is globally asymptotically stable, which can be proved via a linear Lyapunov function. When $f_{\text{crit}} > 0$, the system undergoes a transcritical bifurcation at $f = f_{\text{crit}}$, verified by Sotomayor's theorem. Hopf bifurcation is ruled out by the decoupled structure of the system, which forces the relevant Jacobian trace to remain strictly negative. Ecologically, reproductive suppression and mortality amplification act as amplifying interactions: the combined extinction threshold is strictly lower than the birth-only threshold, while mortality associated with fear alone may lack a finite threshold entirely owing to the saturation of the Holling-Type II response. This dual-pathway interaction is quantified analytically and confirmed by model-variant numerical comparison. All analytical results are corroborated by numerical simulations.

Keywords: amensalism; fear effect; stage structure; global stability; transcritical bifurcation; Lyapunov function

1. Introduction

Amensalism—an asymmetric interaction in which one species is inhibited while the other remains unaffected [1]—is exemplified by allelopathic suppression of understory vegetation by black walnut

trees [2], antibiotic release by *Penicillium* fungi, and trampling of ground-nesting birds by large herbivores. Its mathematical study has attracted considerable recent attention [3–8].

An empirical motivation for incorporating fear effects comes from Xi et al. [9], who documented that in Tibetan alpine meadows, grasshoppers amensalistically suppress grassland caterpillars: the grasshoppers' inadvertent disturbances severely reduced caterpillar feeding time, slowed development, and ultimately reduced egg production. Building on this observation, Chong et al. [10] proposed the first amensalism model with fear effect:

$$\frac{dx}{dt} = x\left(\frac{e_1}{1+k_1y} - (1+k_2y)e_2 - b_1x - c_1y\right), \quad \frac{dy}{dt} = y(a_2 - c_2y), \tag{1.1}$$

where $1/(1+k_1y)$ captures fear-induced birth suppression and $(1+k_2y)$ indicates fear-induced death amplification, with two independent fear coefficients k_1, k_2. They established the local and global stability for the autonomous case using differential inequality theory and the Dulac criterion. Since then, fear effects in amensalism have attracted sustained interest [11–14].

Two limitations of the Chong et al. model motivate the present work. First, it lacks stage structure, treating all individuals of the inhibited species as ecologically equivalent, yet many organisms exhibit distinct juvenile and adult stages with fundamentally different vital rates. Second, the death-fear term $(1+k_2y)e_2$ grows linearly and unboundedly with y, which is ecologically implausible given the physiological ceilings on stress-induced mortality.

A large body of empirical research has established the ecology of fear frameworks. Zanette et al. [15] demonstrated that perceived predation risk alone reduced offspring production by 40% in song sparrows; subsequent studies across diverse taxa—snowshoe hares [16], elk [17], and many others—have corroborated that chronic fear elevates glucocorticoid stress hormones [18], induces vigilance-foraging trade-offs [19], and transmits maternal stress to offspring [20]. Mathematically, Wang et al. [21] formalized fear effects through a Holling-Type II response $\phi(k, y) = 1/(1+ky)$ modifying the prey's birth rates, a framework since extended to group defense [22] and eco-epidemiology [23].

In parallel, stage-structured models were pioneered by Aiello and Freedman [24] for single-species growth with immature and mature stages; extensions to predator-prey systems [25] and delay models [26] followed. Lei [27] proposed a stage-structured amensalism model in which the inhibited species possesses immature (x_1) and mature (x_2) stages:

$$\begin{cases} \dfrac{dx_1}{dt} = \alpha x_2 - \beta x_1 - \delta_1 x_1 - d_1(1-k)x_1y, \\ \dfrac{dx_2}{dt} = \beta x_1 - \delta_2 x_2 - \gamma x_2^2 - d_2(1-k)x_2y, \\ \dfrac{dy}{dt} = y(b_2 - a_2y), \end{cases} \tag{1.2}$$

where $k \in (0,1)$ is a cover proportion. Lei obtained sufficient conditions for the global attractivity of positive and boundary equilibria, but the model considers only direct harmful interactions and omits fear-mediated effects.

While Chong et al. [10] addressed fear in unstructured amensalism and Lei [27] addressed stage structure without fear, the integration of stage structure with fear effects in the amensalism framework remains unexplored. We ask the following questions: can fear alone—independent of direct amensal

harm—drive a stage-structured population to extinction? And do reproductive suppression and mortality amplification interact additively or as amplifying interactions? To answer these questions, we extend Lei's framework by a single fear parameter f with a saturated death-fear term $\delta_2(1 + fy/(1 + fy))$ that approaches the finite ceiling $2\delta_2$, prove the global stability in both regimes via complementary Lyapunov functions, classify the resulting transcritical bifurcation via Sotomayor's theorem, and analytically separate the birth-and-death-associated fear pathways to quantify their amplifying interaction.

The remainder of this paper is organized as follows. Section 2 presents the model's formulation. Section 3 establishes the positivity, boundedness, and equilibrium existence. Section 4 analyzes the local stability. Section 5 proves the global stability via Lyapunov methods. Section 6 provides the bifurcation analysis. Section 7 presents numerical simulations. Section 8 discusses the biological implications, limitations, and future directions.

2. Model formulation

2.1. Ecological motivation

Consider a two-species amensalism system. Species 1 (the inhibited species) possesses a two-stage life history comprising an immature (juvenile) stage x_1 and a mature (adult) stage x_2. Only adults reproduce; juveniles must mature before contributing to reproduction. Both stages experience density-independent natural mortality, and adults additionally experience density-dependent intra-specific competition. Species 2 (the amensal species) follows logistic growth independent of Species 1. The presence of Species 2 exerts dual negative effects on Species 1: Direct harm through physical or chemical mechanisms, and fear effects through perceived threats inducing chronic physiological stress.

The ecological rationale for directing fear effects toward adult mortality rather than juvenile mortality is threefold. First, adults are the primary perceivers of threat cues: The physiological stress cascade (i.e., activation of the hypothalamic–pituitary–adrenal axis, elevated glucocorticoids, immunosuppression) is initiated in adults that directly detect the amensal species, making adult survival the natural target of fear-amplified mortality. Second, fear already suppresses juvenile recruitment indirectly through reduced adult reproductive output (the $\alpha/(1 + fy)$ term); introducing an additional fear-induced juvenile mortality term would effectively double-count the same ecological phenomenon via two different channels. Third, Zanette et al. [15] showed empirically that perceived predation risk primarily reduces offspring number rather than offspring survival, providing direct experimental support for confining fear effects to the reproductive and adult-survival pathways.

2.2. The model

We propose the following three-dimensional system:

$$\begin{aligned}
\frac{dx_1}{dt} &= \frac{\alpha}{1+fy}\, x_2 - \beta x_1 - \delta_1 x_1 - d_1 x_1 y, \\
\frac{dx_2}{dt} &= \beta x_1 - \delta_2\left(1 + \frac{fy}{1+fy}\right) x_2 - \gamma x_2^2 - d_2 x_2 y, \\
\frac{dy}{dt} &= y(b - ay),
\end{aligned} \tag{2.1}$$

with the initial conditions $x_1(0) \geq 0$, $x_2(0) \geq 0$, $y(0) \geq 0$. All parameters are positive, with interpretations given in Table 1.

Table 1. Parameter definitions and ecological interpretations.

Parameter	Definition	Unit
α	Per capita birth rate of adults (in the absence of fear)	time^{-1}
β	Maturation rate from juvenile to adult	time^{-1}
δ_1	Natural mortality rate of juveniles	time^{-1}
δ_2	Natural mortality rate of adults (in the absence of fear)	time^{-1}
γ	Intra-specific competition coefficient among adults	density^{-1}·time^{-1}
d_1	Direct amensal harm coefficient on juveniles	density^{-1}·time^{-1}
d_2	Direct amensal harm coefficient on adults	density^{-1}·time^{-1}
b	Intrinsic growth rate of the amensal species	time^{-1}
a	Intra-specific competition coefficient of the amensal species	density^{-1}·time^{-1}
$\boldsymbol{f}$	**Fear effect coefficient**	**density^{-1}**†

†As a composite parameter, f is estimated from empirical fitting of the Holling-type II response $\phi(y) = fy/(1+fy)$ rather than measured directly.

2.3. Fear effect mechanisms

Equation (2.1) differs from Lei [27] in exactly two terms, both governed by the same fear parameter f. The birth rate is modified from α to $\alpha/(1+fy)$, capturing reproductive suppression. The adult mortality rate is modified from δ_2 to $\delta_2(1 + \frac{fy}{1+fy})$, capturing fear-amplified mortality. Equivalently, $\delta_2(1 + \frac{fy}{1+fy}) = \delta_2\frac{1+2fy}{1+fy}$, which makes it transparent that the total adult death rate interpolates between δ_2 (at $y = 0$) and $2\delta_2$ (as $y \to \infty$).

Defining the normalized fear intensity $\phi(y) := fy/(1+fy) \in [0, 1)$, the two fear-modified rates adopt the compact forms $\alpha \mapsto \alpha(1-\phi)$ and $\delta_2 \mapsto \delta_2(1+\phi)$, revealing that fear suppresses reproduction toward zero while amplifying the total adult mortality toward a finite ceiling of $2\delta_2$.

For comparison, the death-fear term in Chong et al. [10] took the linear form $(1 + k_2 y)e_2$, which grows without bound as $y \to \infty$. Our formulation $\delta_2(1 + \frac{fy}{1+fy})$ saturates at $2\delta_2$, reflecting the physiological ceiling on stress-induced mortality. Moreover, whereas Chong et al. used two independent fear parameters (k_1, k_2), we adopt a single parameter f, treating fear sensitivity as a unified trait; this simplifies the model and yields an explicit fear threshold derived in Section 3.

The fear response function $\phi(y) := fy/(1+fy)$ satisfies: $\phi(0) = 0$, $\phi(y) \to 1$ as $y \to \infty$, $\phi'(y) = f/(1+fy)^2 > 0$, and $\phi''(y) < 0$.

Remark 2.1 (Structural asymmetry of the two fear pathways). Although both fear effects are governed by the same parameter f (and consequently by the same ϕ), they enter the model through functionally *asymmetric* channels.

- **Birth suppression:** $\alpha \mapsto \alpha(1-\phi)$. As $\phi \to 1$ (intense fear), the birth rate is driven to zero — a complete reproductive shutdown.
- **Mortality amplification:** $\delta_2 \mapsto \delta_2(1+\phi)$. As $\phi \to 1$, the total adult death rate at most doubles, saturating at the finite ceiling $2\delta_2$.

This asymmetry has a clear biological interpretation: As fear intensifies, the birth rate can be driven to zero, while the mortality rate at most doubles. Consequently, reproductive suppression is the primary route to extinction, with mortality amplification playing a secondary, saturating role. This asymmetry underlies the dual-pathway mechanism analysed in Section 6.2 and confirmed numerically in Section 7.

3. Preliminaries

3.1. Positivity and boundedness

Proposition 3.1 (Positivity)**.** *For any non-negative initial conditions* $(x_1(0), x_2(0), y(0)) \in \mathbb{R}^3_+$*, the solution of system* (2.1) *remains non-negative for all* $t > 0$*.*

Proof. From the third equation, the logistic dynamics admit the explicit solution

$$y(t) = \frac{b\,y(0)}{a\,y(0) + (b - a\,y(0))\,e^{-bt}} \geq 0, \tag{3.1}$$

which is manifestly non-negative for all $t \geq 0$ and converges monotonically to $y^* = b/a$ whenever $y(0) > 0$. At $x_1 = 0$, $\dot{x}_1 = \frac{\alpha}{1+fy} x_2 \geq 0$; at $x_2 = 0$, $\dot{x}_2 = \beta x_1 \geq 0$. By the positive invariance theorem for ODEs (see, e.g., Theorem 2.1 in Smith [29]), $\mathbb{R}^3_+$ is positively invariant.

Proposition 3.2 (Boundedness)**.** *All solutions of system* (2.1) *with non-negative initial conditions are bounded for all* $t \geq 0$*.*

Proof. The logistic equation $\dot{y} = y(b - ay)$ admits the explicit solution (3.1), yielding

$$0 \leq y(t) \leq M_y := \max\{y(0),\, b/a\}, \qquad \forall\, t \geq 0. \tag{3.2}$$

From (2.1), using the elementary bounds $\frac{1}{1+fy} \leq 1$, $\delta_2(1 + \frac{fy}{1+fy}) \geq \delta_2$, and dropping the non-positive terms $-d_1 x_1 y$, $-d_2 x_2 y$, we obtain the componentwise upper estimates

$$\frac{dx_1}{dt} \leq \alpha x_2 - (\beta + \delta_1)x_1, \qquad \frac{dx_2}{dt} \leq \beta x_1 - \delta_2 x_2 - \gamma x_2^2. \tag{3.3}$$

Consider the auxiliary planar system

$$\frac{du_1}{dt} = \alpha u_2 - (\beta + \delta_1)u_1, \qquad \frac{du_2}{dt} = \beta u_1 - \delta_2 u_2 - \gamma u_2^2, \tag{3.4}$$

with $u_i(0) = x_i(0)$. System (3.4) is precisely the stage-structured subsystem of Lei [27] with zero cover ($k = 0$). Lemma 2.1 of [27] establishes the global asymptotic stability of either the trivial equilibrium (when $\alpha\beta < \delta_2(\beta + \delta_1)$) or the positive equilibrium (when $\alpha\beta > \delta_2(\beta + \delta_1)$) for this subsystem. Global stability implies, in particular, that all solutions are uniformly bounded.

The Jacobian of (3.4) has non-negative off-diagonal entries ($\alpha > 0$, $\beta > 0$); hence the system is cooperative on $\mathbb{R}^2_+$. By the Kamke–Müller comparison theorem for cooperative systems (see, e.g., [29], Theorem 3.4), $x_i(t) \le u_i(t)$ for all $t \ge 0$ and $i = 1, 2$.

Since $(u_1(t), u_2(t))$ is bounded, $(x_1(t), x_2(t))$ is bounded.

3.2. Asymptotic autonomy and dimensional reduction

If $y(0) = 0$, then $y(t) \equiv 0$ and the system reduces to a two-dimensional model on $\{y = 0\}$. If $y(0) > 0$, then $\lim_{t\to\infty} y(t) = b/a := y^*$. Since all solutions are bounded (Proposition 3.2), the forward orbits are precompact and, by the theory of asymptotically autonomous systems [28], the (x_1, x_2)-subsystem is asymptotically autonomous with the limiting system:

$$\begin{aligned} \frac{dx_1}{dt} &= \tilde{\alpha}\, x_2 - \tilde{B}\, x_1, \\ \frac{dx_2}{dt} &= \beta x_1 - \tilde{C}\, x_2 - \gamma x_2^2, \end{aligned} \tag{3.5}$$

where the effective parameters are defined as

$$\begin{aligned} \Phi &:= \frac{fy^*}{1 + fy^*} = \phi(y^*) \in [0, 1), \\ \tilde{\alpha} &:= \frac{\alpha}{1 + fy^*} = \alpha(1 - \Phi), \\ \tilde{B} &:= \beta + \delta_1 + d_1 y^*, \\ \tilde{C} &:= \delta_2(1 + \Phi) + d_2 y^*. \end{aligned} \tag{3.6}$$

Thus Φ is simply the normalized fear intensity ϕ (introduced in Section 2.3) evaluated at the amensal carrying capacity y^*. The three effective parameters fully encode the fear-modified birth rate ($\tilde{\alpha}$), the total juvenile removal rate ($\tilde{B}$), and the total adult removal rate ($\tilde{C}$) in the asymptotic regime. Note the useful identity $\frac{1}{1+fy^*} = 1 - \Phi$, which follows directly from the definition of Φ.

3.3. Equilibrium points

System (2.1) possesses at most four equilibrium points, obtained by setting all the time derivatives to zero.

(i) $E_0 = (0, 0, 0)$: The trivial equilibrium, which always exists.

(ii) $E_1 = (x_1^*, x_2^*, 0)$: The boundary equilibrium on the $\{y = 0\}$ plane. Setting $y = 0$ in (2.1) and solving $\dot{x}_1 = \dot{x}_2 = 0$ yields

$$x_2^* = \frac{1}{\gamma}\left(\frac{\alpha\beta}{\beta + \delta_1} - \delta_2\right), \qquad x_1^* = \frac{\alpha}{\beta + \delta_1}\, x_2^*. \tag{3.7}$$

Define the net reproduction number in the absence of the amensal species as

$$\mathcal{N}_0 := \frac{\alpha\beta}{(\beta + \delta_1)\delta_2}. \tag{3.8}$$

In keeping with the ecological terminology for stage-structured models, $\mathcal{N}_0$ is a net reproduction number (the product of per capita fertility $\alpha/(\beta + \delta_1)$ and the maturation probability β/δ_2) rather than an epidemiological basic reproduction number in the strict sense. Then E_1 exists in the positive orthant if and only if $\mathcal{N}_0 > 1$.

(iii) $E_2 = (0, 0, y^*)$: The Species 1 extinction equilibrium, where $y^* = b/a$. This equilibrium always exists.

(iv) $E^* = (x_1^{**}, x_2^{**}, y^*)$: The coexistence equilibrium. Solving $\dot{x}_1 = \dot{x}_2 = 0$ with $y = y^*$ in the limiting system (3.5) gives

$$x_2^{**} = \frac{1}{\gamma}\Big(\frac{\tilde{\alpha}\beta}{\tilde{B}} - \tilde{C}\Big), \qquad x_1^{**} = \frac{\tilde{\alpha}}{\tilde{B}}\, x_2^{**}. \tag{3.9}$$

Define the net reproduction number under fear as

$$\mathcal{R}_{\text{fear}} := \frac{\tilde{\alpha}\beta}{\tilde{B}\tilde{C}} = \frac{\alpha\beta(1 - \Phi)}{\tilde{B}\,[\,\delta_2(1 + \Phi) + d_2 y^*\,]}. \tag{3.10}$$

Comparing $\mathcal{R}_{\text{fear}}$ with $\mathcal{N}_0$ reveals the dual action of fear: The numerator is attenuated by the factor $(1 - \Phi)$ (birth suppression, via $\tilde{\alpha}$), while the denominator inherits the term $\delta_2(1 + \Phi) + d_2 y^*$ (mortality amplification, via $\tilde{C}$), in addition to the direct-amensal contribution $d_1 y^*$ already present in $\tilde{B}$. Both modifications push $\mathcal{R}_{\text{fear}}$ in the same direction (toward values below 1) and they do so through the single scalar $\Phi = \phi(y^*)$. Then E^* exists in the positive orthant if and only if $\mathcal{R}_{\text{fear}} > 1$.

Theorem 3.3 (Existence of E^* —the fear threshold)**.** *Define the critical fear coefficient*

$$f_{\text{crit}} := \frac{\dfrac{\alpha\beta}{\beta + \delta_1 + d_1 y^*} - \delta_2 - d_2 y^*}{y^*(2\delta_2 + d_2 y^*)}. \tag{3.11}$$

Assume $\mathcal{N}_0 > 1$ (so that Species 1 can persist in the absence of the amensal species). Then the following trichotomy holds.

(i) If $f_{\text{crit}} > 0$ and $0 \le f < f_{\text{crit}}$, then E^* exists in the positive orthant (equivalently, $\mathcal{R}_{fear} > 1$).

(ii) If $f_{\text{crit}} > 0$ and $f \ge f_{\text{crit}}$, then E^* does not exist in the positive orthant (equivalently, $\mathcal{R}_{fear} \le 1$).

(iii) If $f_{\text{crit}} \le 0$, then E^* never exists in the positive orthant for any $f \ge 0$: The direct amensal harm alone (d_1, d_2) is sufficiently severe that even zero fear cannot sustain coexistence, and $\mathcal{R}_{fear} \le 1$ for all $f \ge 0$.

Proof. From (3.10), the condition $\mathcal{R}_{\text{fear}} > 1$ is equivalent to

$$\tilde{\alpha}\beta > \tilde{B}\tilde{C}. \tag{3.12}$$

Substituting $\tilde{\alpha} = \alpha(1 - \Phi)$ and $\tilde{C} = \delta_2(1 + \Phi) + d_2 y^*$ from (3.6) yields

$$\alpha\beta(1 - \Phi) > \tilde{B}[\delta_2(1 + \Phi) + d_2 y^*]. \tag{3.13}$$

Expanding and collecting the terms involving Φ on the right-hand side yields:

$$\begin{aligned} \alpha\beta - \alpha\beta\Phi &> \tilde{B}\delta_2 + \tilde{B}\delta_2\Phi + \tilde{B}d_2 y^* \\ \alpha\beta - \tilde{B}(\delta_2 + d_2 y^*) &> \Phi(\alpha\beta + \tilde{B}\delta_2). \end{aligned} \tag{3.14}$$

Since $\alpha\beta + \tilde{B}\delta_2 > 0$, we obtain the equivalent condition

$$\Phi < \frac{\alpha\beta - \tilde{B}(\delta_2 + d_2 y^*)}{\alpha\beta + \tilde{B}\delta_2} =: \Phi_{\max}. \tag{3.15}$$

Now recall the defining relation $\Phi = fy^*/(1 + fy^*)$, which is equivalent to $f = \Phi/[y^*(1 - \Phi)]$. Because the map $\Phi \mapsto \Phi/[y^*(1 - \Phi)]$ is strictly increasing on $[0, 1)$, the inequality $\Phi < \Phi_{\max}$ is equivalent to $f < \Phi_{\max}/[y^*(1 - \Phi_{\max})]$. Substituting the expression for $\Phi_{\max}$, we have:

$$\begin{aligned} f &< \frac{1}{y^*} \frac{\dfrac{\alpha\beta - \tilde{B}(\delta_2 + d_2 y^*)}{\alpha\beta + \tilde{B}\delta_2}}{1 - \dfrac{\alpha\beta - \tilde{B}(\delta_2 + d_2 y^*)}{\alpha\beta + \tilde{B}\delta_2}} \\ &= \frac{1}{y^*} \frac{\alpha\beta - \tilde{B}(\delta_2 + d_2 y^*)}{\alpha\beta + \tilde{B}\delta_2 - \alpha\beta + \tilde{B}(\delta_2 + d_2 y^*)} \\ &= \frac{\alpha\beta - \tilde{B}(\delta_2 + d_2 y^*)}{\tilde{B}\, y^* (2\delta_2 + d_2 y^*)} \\ &= \frac{\dfrac{\alpha\beta}{\tilde{B}} - \delta_2 - d_2 y^*}{y^*(2\delta_2 + d_2 y^*)} =: f_{\text{crit}}. \end{aligned} \tag{3.16}$$

Recalling $\tilde{B} = \beta + \delta_1 + d_1 y^*$, the right-hand side is precisely f_{crit} as defined in (3.11).

Corollary 3.4 (Biological trichotomy)**.** *The sign of f_{crit} determines two fundamentally different regimes.*

- ***Positive threshold*** *($f_{\text{crit}} > 0$). Then $\alpha\beta/\tilde{B} > \delta_2 + d_2 y^*$, so that in the absence of fear ($f = 0$, $\Phi = 0$) we have $\mathcal{R}_{fear} > 1$, and E^* exists. As f increases, Φ increases, $\mathcal{R}_{fear}$ decreases monotonically, and E^* persists as long as $f < f_{\text{crit}}$ (equivalently $\mathcal{R}_{fear} > 1$). When $f \geq f_{\text{crit}}$ ($\mathcal{R}_{fear} \leq 1$), $x_2^{**} \leq 0$ and E^* leaves the positive orthant.*
- ***Non-positive threshold*** *($f_{\text{crit}} \leq 0$). Then $\alpha\beta/\tilde{B} \leq \delta_2 + d_2 y^*$, so that even at $f = 0$, we have $\mathcal{R}_{fear} \leq 1$. Since $\mathcal{R}_{fear}$ is strictly decreasing in f, it remains ≤ 1 for all $f \geq 0$, and E^* never enters the positive orthant. In this regime, direct amensal harm alone is sufficient to preclude coexistence.*

Remark 3.5 (Structure of f_{crit}). The derivation above clarifies the structure of f_{crit}.

- **Numerator.** $\frac{\alpha\beta}{\tilde{B}} - (\delta_2 + d_2 y^*)$ is the net growth capacity of Species 1 at the amensal density y^* in the absence of fear ($f = 0$).
- **Denominator.** $y^*(2\delta_2 + d_2 y^*)$ arises from clearing denominators in the expression for $\mathcal{R}_{\text{fear}}$. Its component $2\delta_2$ reflects the saturation ceiling of fear-amplified mortality ($\delta_2 \to 2\delta_2$ as $\phi \to 1$), while $d_2 y^*$ is the direct amensal mortality at density y^*.
- **Threshold logic.** The condition $f < f_{\text{crit}}$ is equivalent to $\Phi < \Phi_{\max}$ with $\Phi_{\max} = (\alpha\beta - \tilde{B}(\delta_2 + d_2 y^*))/(\alpha\beta + \tilde{B}\delta_2)$. Because f and Φ are monotonically related via $\Phi = fy^*/(1 + fy^*)$, the same biological threshold can be expressed in either variable.

4. Local stability analysis

The Jacobian matrix of system (2.1) at any point (x_1, x_2, y) is

$$J(x_1, x_2, y) = \begin{bmatrix} -(\beta + \delta_1 + d_1 y) & \dfrac{\alpha}{1+fy} & -\dfrac{\alpha f}{(1+fy)^2} x_2 - d_1 x_1 \\ \beta & -\delta_2\left(1 + \dfrac{fy}{1+fy}\right) - 2\gamma x_2 - d_2 y & -\dfrac{\delta_2 f}{(1+fy)^2} x_2 - d_2 x_2 \\ 0 & 0 & b - 2ay \end{bmatrix}. \tag{4.1}$$

A crucial structural observation is that J is block upper-triangular at every point in phase space—a direct consequence of the amensal species y being unaffected by Species 1. Hence one eigenvalue is always

$$\lambda_3 = b - 2ay, \tag{4.2}$$

and the remaining two eigenvalues are those of the 2×2 submatrix

$$J_2(x_1, x_2, y) = \begin{bmatrix} -(\beta + \delta_1 + d_1 y) & \dfrac{\alpha}{1+fy} \\ \beta & -\delta_2\left(1 + \dfrac{fy}{1+fy}\right) - 2\gamma x_2 - d_2 y \end{bmatrix}. \tag{4.3}$$

Because all parameters are positive and $(x_1, x_2, y) \in \mathbb{R}^3_+$ (Proposition 3.1), the trace of J_2 is strictly negative

$$\operatorname{tr} J_2 = -(\beta + \delta_1 + d_1 y) - \delta_2\left(1 + \frac{fy}{1+fy}\right) - 2\gamma x_2 - d_2 y \; < \; 0, \tag{4.4}$$

a property that plays a key role in precluding Hopf bifurcation (Section 4.5). We now evaluate J at each equilibrium.

4.1. Stability of $E_0 = (0, 0, 0)$

Theorem 4.1 (Stability of E_0)**.** *The trivial equilibrium E_0 is always unstable. For $\mathcal{N}_0 \neq 1$, it is a saddle; at $\mathcal{N}_0 = 1$, E_0 has a one-dimensional center manifold within $\{y = 0\}$ and coincides with E_1, prefiguring the transcritical structure of the full system.*

Proof. At E_0, substituting $x_1 = x_2 = y = 0$ into (4.1) yields

$$J(E_0) = \begin{bmatrix} -(\beta + \delta_1) & \alpha & 0 \\ \beta & -\delta_2 & 0 \\ 0 & 0 & b \end{bmatrix}, \tag{4.5}$$

so $\lambda_3 = b > 0$. The 2×2 submatrix has the trace $-(\beta + \delta_1 + \delta_2) < 0$ and the determinant $\Delta = \delta_2(\beta + \delta_1)(1 - \mathcal{N}_0)$. If $\mathcal{N}_0 < 1$, then $\Delta > 0$ and $J_2(E_0)$ has two eigenvalues with negative real parts; E_0 is a saddle with a two-dimensional (2D) stable manifold. If $\mathcal{N}_0 > 1$, then $\Delta < 0$ giving one positive and one negative real root; together with $\lambda_3 > 0$, E_0 has a one-dimensional (1D) stable manifold. If $\mathcal{N}_0 = 1$, then $\Delta = 0$; eigenvalues are 0, $-(\beta + \delta_1 + \delta_2)$, and $b > 0$—a center manifold within $\{y = 0\}$ where E_0 and E_1 coalesce. In all cases, $\lambda_3 = b > 0$ guarantees instability.

4.2. Stability of $E_1 = (x_1^*, x_2^*, 0)$

Theorem 4.2 (Stability of E_1)**.** *Assume $\mathcal{N}_0 > 1$ so that E_1 exists. Then E_1 is always a saddle point: its restriction to the invariant plane $\{y = 0\}$ is a stable node or focus, but the y-direction is always repelling.*

Proof. At E_1, $y = 0$ and the $(3, 3)$ entry of (4.1) is $b > 0$. Hence, $\lambda_3 = b > 0$, and E_1 possesses a 1D unstable manifold transverse to $\{y = 0\}$. Within $\{y = 0\}$, the 2×2 submatrix has a trace $-(\beta + \delta_1 + \delta_2 + 2\gamma x_2^*) < 0$ and, using the equilibrium relation $\alpha\beta = (\beta + \delta_1)(\delta_2 + \gamma x_2^*)$, and the determinant $(\beta + \delta_1)\gamma x_2^* > 0$; thus both eigenvalues of $J_2(E_1)$ have negative real parts. Consequently, E_1 is a saddle with a 2D stable manifold (the plane $\{y = 0\}$) and a 1D unstable manifold.

4.3. Stability of $E_2 = (0, 0, y^*)$

Theorem 4.3 (Stability of E_2)**.** *Let $E_2 = (0, 0, y^*)$ with $y^* = b/a$. Then:*

(i) If $f < f_{\text{crit}}$ (equivalently $\mathcal{R}_{fear} > 1$), then E_2 is a saddle point.

(ii) If $f = f_{\text{crit}}$ (equivalently $\mathcal{R}_{fear} = 1$), then $J(E_2)$ has a simple zero eigenvalue while the other two eigenvalues are negative.

(iii) If $f > f_{\text{crit}}$ (equivalently $\mathcal{R}_{fear} < 1$), then E_2 is locally asymptotically stable.

Proof. At E_2, $x_1 = x_2 = 0$, $y = y^*$, and $b - 2ay^* = -b$. Using the effective parameters (3.6), we have

$$J(E_2) = \begin{bmatrix} -\tilde{B} & \tilde{\alpha} & 0 \\ \beta & -\tilde{C} & 0 \\ 0 & 0 & -b \end{bmatrix}, \tag{4.6}$$

yielding $\lambda_3 = -b < 0$. The 2×2 submatrix has the characteristic equation

$$\lambda^2 + (\tilde{B} + \tilde{C})\lambda + \tilde{B}\tilde{C}(1 - \mathcal{R}_{\text{fear}}) = 0, \tag{4.7}$$

with the trace $T_2 = -(\tilde{B} + \tilde{C}) < 0$ and the determinant $\Delta_2 = \tilde{B}\tilde{C}(1 - \mathcal{R}_{\text{fear}})$.

Case (i): $f < f_{\text{crit}}$ *(*$\mathcal{R}_{fear} > 1$*).* $\Delta_2 < 0$; the quadratic has two real roots of the opposite sign. Together with $\lambda_3 < 0$, E_2 is a saddle with a 2D stable manifold.

Case (ii): $f = f_{\text{crit}}$ *(*$\mathcal{R}_{fear} = 1$*).* $\Delta_2 = 0$; the eigenvalues are 0, $-(\tilde{B} + \tilde{C}) < 0$, and $-b < 0$. The simple zero eigenvalue signals a bifurcation (proved transcritical in Section 6).

Case (iii): $f > f_{\text{crit}}$ *(*$\mathcal{R}_{fear} < 1$*).* $\Delta_2 > 0$; with $T_2 < 0$, both roots of (4.7) have negative real parts, so all three eigenvalues are negative and E_2 is locally asymptotically stable.

Remark 4.4. From (4.7), the eigenvalues of $J_2(E_2)$ are $\lambda_{1,2} = \frac{1}{2}[-(\tilde{B} + \tilde{C}) \pm \sqrt{(\tilde{B} - \tilde{C})^2 + 4\tilde{B}\tilde{C}\,\mathcal{R}_{\text{fear}}}\,]$, from which one verifies directly that the crossing eigenvalue is positive for $\mathcal{R}_{\text{fear}} > 1$, zero at $\mathcal{R}_{\text{fear}} = 1$, and negative for $\mathcal{R}_{\text{fear}} < 1$.

4.4. Stability of $E^* = (x_1^{**}, x_2^{**}, y^*)$

Theorem 4.5 (Stability of E^*)**.** *Assume* $\mathcal{N}_0 > 1$ *and* $f < f_{\text{crit}}$ *(so that* E^* *exists in the positive orthant). Then* E^* *is locally asymptotically stable.*

Proof. At E^*, $y = y^*$ and $b - 2ay^* = -b < 0$, so $\lambda_3 = -b < 0$. The 2×2 submatrix is

$$J_2(E^*) = \begin{bmatrix} -\tilde{B} & \tilde{\alpha} \\ \beta & -\tilde{C} - 2\gamma x_2^{**} \end{bmatrix}, \tag{4.8}$$

with characteristic equation $\lambda^2 + P\lambda + Q = 0$, where $P = \tilde{B} + \tilde{C} + 2\gamma x_2^{**} > 0$ and $Q = \tilde{B}(\tilde{C} + 2\gamma x_2^{**}) - \tilde{\alpha}\beta$. Using the equilibrium relation $\tilde{\alpha}\beta = \tilde{B}(\tilde{C} + \gamma x_2^{**})$ from (3.9),

$$Q = \tilde{B}(\tilde{C} + 2\gamma x_2^{**}) - \tilde{B}(\tilde{C} + \gamma x_2^{**}) = \tilde{B}\gamma x_2^{**} > 0. \tag{4.9}$$

For a 2×2 real matrix, $P > 0$ and $Q > 0$ are necessary and sufficient for both eigenvalues to have negative real parts. Hence, all three eigenvalues of $J(E^*)$ satisfy $\text{Re}(\lambda) < 0$, and E^* is locally asymptotically stable.

4.5. Absence of Hopf bifurcation

Remark 4.6 (Absence of Hopf bifurcation). A Hopf bifurcation requires a pair of purely imaginary eigenvalues $\lambda = \pm i\omega$ ($\omega > 0$). For system (2.1), this is structurally precluded. First, the block upper-triangular form of J confines any purely imaginary pair to the 2×2 submatrix J_2 because $\lambda_3 = b - 2ay$ is always real (equal to b at E_0, E_1 and $-b$ at E_2, E^*). Second, for a 2×2 real matrix, a purely imaginary pair requires a zero trace. The trace of J_2 is strictly negative at every admissible equilibrium: $-(\beta + \delta_1 + \delta_2) < 0$ at E_0, $-(\beta + \delta_1 + \delta_2 + 2\gamma x_2^*) < 0$ at E_1, $-(\tilde{B} + \tilde{C}) < 0$ at E_2, and $-(\tilde{B} + \tilde{C} + 2\gamma x_2^{**}) < 0$ at E^*. Thus no parameter configuration can produce a purely imaginary pair, and Hopf bifurcation is impossible. The same structural obstruction applies to the autonomous model of Chong et al. [10].

5. Global stability analysis

5.1. Asymptotic autonomy reduction

The logistic equation $\dot{y} = y(b - ay)$ is independent of x_1, x_2 and satisfies $\lim_{t\to\infty} y(t) = y^* = b/a$ for any $y(0) > 0$. Consequently, system (2.1) is asymptotically autonomous with the limiting planar system

$$\frac{dx_1}{dt} = \tilde{\alpha}x_2 - \tilde{B}x_1, \tag{5.1a}$$

$$\frac{dx_2}{dt} = \beta x_1 - \tilde{C}x_2 - \gamma x_2^2, \tag{5.1b}$$

where $\tilde{\alpha}, \tilde{B}, \tilde{C}$ are the effective constants (3.6). All solutions of the full system are bounded (Proposition 3.2), and hence their forward orbits are precompact.

Verification of Thieme's hypothesis. Let $K \subset \mathbb{R}^2_+$ be compact. For $(x_1, x_2) \in K$ and $t \geq 0$, the (x_1, x_2)-subsystem of (2.1) is

$$\dot{x}_1 = \frac{\alpha}{1 + fy(t)}\, x_2 - (\beta + \delta_1 + d_1 y(t))x_1, \tag{5.2}$$

$$\dot{x}_2 = \beta x_1 - \delta_2\Big(1 + \frac{fy(t)}{1 + fy(t)}\Big)x_2 - \gamma x_2^2 - d_2 y(t)x_2. \tag{5.3}$$

Its deviation from the limiting field (5.1) involves

$$\Delta_\alpha(t) := \frac{\alpha}{1 + fy(t)} - \tilde{\alpha}, \qquad \Delta_\delta(t) := \delta_2\Big(1 + \frac{fy(t)}{1 + fy(t)}\Big) - \tilde{C} + d_2 y^*, \tag{5.4}$$

together with $y(t) - y^*$ in the terms $d_1 y(t)x_1$ and $d_2 y(t)x_2$. Since $y(t) \to y^*$ as $t \to \infty$, the logistic solution satisfies $|y(t) - y^*| \leq Ce^{-bt}$ for some $C > 0$ and all $t \geq 0$; hence

$$|\Delta_\alpha(t)| \leq \alpha f C e^{-bt}, \qquad |\Delta_\delta(t)| \leq 2\delta_2 f C e^{-bt}, \tag{5.5}$$

and the perturbation to the vector field decays to zero exponentially and uniformly in $(x_1, x_2) \in K$. Because the limiting field (5.1) is Lipschitz on K, the hypotheses of Thieme [28, Theorem 4.1] are satisfied.

Applicability of Thieme's theorem. Theorem 4.1 of [28] states that if the forward orbit of an asymptotically autonomous system is precompact, its ω-limit set is non-empty, compact, invariant under the limiting system, and attracts the orbit. For system (2.1): (i) All solutions with $y(0) > 0$ are bounded (Proposition 3.2) and hence are precompact; (ii) the limiting planar system (5.1) possesses exactly one globally asymptotically stable equilibrium in $\mathbb{R}^2_+$ in each parameter regime—$(0, 0)$ when $f \geq f_{\text{crit}}$ and (x_1^{**}, x_2^{**}) when $f < f_{\text{crit}}$, as proved in Sections 5.3 and 5.4; and (iii) because the limiting system is planar and its equilibria are hyperbolic (except at $f = f_{\text{crit}}$, a transcritical point), the Poincaré–Bendixson trichotomy together with the Lyapunov functions constructed below rules out periodic orbits and other non-trivial ω-limit sets. Consequently, the global asymptotic stability of an equilibrium of (5.1) lifts to the corresponding equilibrium of (2.1). It therefore suffices to analyze the planar system (5.1).

5.2. Positive invariance and interior penetration

Lemma 5.1 (Positive invariance and interior penetration)**.** *For system* (5.1)*:*

(i) $\mathbb{R}^2_+$ *is positively invariant.*

(ii) If $(x_1(0), x_2(0)) \neq (0,0)$*, then* $x_1(t) > 0$ *and* $x_2(t) > 0$ *for all* $t > 0$*.*

Proof. (i) On $x_1 = 0$ ($x_2 \geq 0$), $\dot{x}_1 = \tilde{\alpha} x_2 \geq 0$; on $x_2 = 0$ ($x_1 \geq 0$), $\dot{x}_2 = \beta x_1 \geq 0$. By tangency criterion [29], no trajectory exits through either axis.

(ii) For x_1: If $x_1(0) > 0$, the variation-of-constants formula $x_1(t) = x_1(0)e^{-\tilde{B}t} + \tilde{\alpha} \int_0^t e^{-\tilde{B}(t-s)} x_2(s)\, ds$ is strictly positive. If $x_1(0) = 0$ and $x_2(0) > 0$, then $\dot{x}_1(0) = \tilde{\alpha} x_2(0) > 0$, so x_1 becomes positive immediately.

For x_2: If $x_2(0) > 0$, then $\dot{x}_2 = \beta x_1 - \tilde{C} x_2 - \gamma x_2^2 \geq -\tilde{C} x_2 - \gamma x_2^2$. The comparison initial value problem (IVP) $\dot{z} = -\tilde{C} z - \gamma z^2$, $z(0) = x_2(0) > 0$ has the strictly positive solution $z(t) = x_2(0)e^{-\tilde{C}t}/(1 + \frac{\gamma x_2(0)}{\tilde{C}}(1 - e^{-\tilde{C}t}))$; by the comparison principle [30], $x_2(t) \geq z(t) > 0$. If $x_2(0) = 0$ and $x_1(0) > 0$, then $\dot{x}_2(0) = \beta x_1(0) > 0$ and x_2 becomes positive immediately.

Thus, whenever $(x_1(0), x_2(0)) \neq (0,0)$, both components enter $\operatorname{int} \mathbb{R}^2_+$ and remain there for all $t > 0$. By shifting the time origin to any $t_0 > 0$, we may assume, without loss of generality, that the initial condition lies in $\operatorname{int} \mathbb{R}^2_+$ for the Lyapunov analysis that follows.

5.3. Global stability of the extinction equilibrium

Theorem 5.2. *Assume* $f \geq f_{\text{crit}}$*. Then* $E_2 = (0, 0, y^*)$ *is globally asymptotically stable for all solutions with* $y(0) > 0$*.*

Proof. By asymptotic autonomy, it suffices to show that $(0, 0)$ is globally asymptotically stable for (5.1). Let

$$W(x_1, x_2) = \beta x_1 + \tilde{B} x_2, \tag{5.6}$$

which is C^1, positive for $(x_1, x_2) \neq (0, 0)$, $W(0, 0) = 0$, and radially unbounded. Differentiating along (5.1), we have

$$\frac{dW}{dt} = \beta(\tilde{\alpha} x_2 - \tilde{B} x_1) + \tilde{B}(\beta x_1 - \tilde{C} x_2 - \gamma x_2^2) = (\beta\tilde{\alpha} - \tilde{B}\tilde{C}) x_2 - \tilde{B}\gamma x_2^2. \tag{5.7}$$

The x_1 cross-terms cancel by construction: The weights β and $\tilde{B}$ are chosen precisely so that $\beta\tilde{B}x_1 = \tilde{B}\beta x_1$.

From Theorem 4.3, $f \geq f_{\text{crit}}$ gives $\mathcal{R}_{\text{fear}} \leq 1$, and hence $\beta\tilde{\alpha} - \tilde{B}\tilde{C} \leq 0$ (this is strict when $f > f_{\text{crit}}$, zero when $f = f_{\text{crit}}$). Therefore $\dot{W} \leq 0$, with equality if and only if (iff) $x_2 = 0$. The largest invariant subset of $\{\dot{W} = 0\}$ is $\{(0, 0)\}$, because $x_2 \equiv 0$ forces $\dot{x}_2 = \beta x_1 = 0$, and hence $x_1 = 0$.

Boundedness of orbits follows from Proposition 3.2 by projection. LaSalle's invariance principle [31, 32] yields $\lim_{t\to\infty}(x_1(t), x_2(t)) = (0, 0)$ for every initial condition in $\mathbb{R}^2_+$. Thieme's theorem [28] lifts this to global asymptotic stability of E_2 for the full system.

At the bifurcation value $f = f_{\text{crit}}$, $\dot{W} = -\tilde{B}\gamma x_2^2 \leq 0$ still holds, so E_2 is globally asymptotically stable at the bifurcation point itself, consistent with the transcritical nature proved in Section 6.

5.4. Global stability of the coexistence equilibrium

Theorem 5.3. *Assume* $f < f_{\text{crit}}$ *(equivalently* $\mathcal{R}_{fear} > 1$*). Then* $E^* = (x_1^{**}, x_2^{**}, y^*)$ *is globally asymptotically stable for all solutions with* $y(0) > 0$ *and* $x_1(0) + x_2(0) > 0$*.*

Proof. By asymptotic autonomy and Lemma 5.1(ii), it suffices to prove that (x_1^{**}, x_2^{**}) is globally asymptotically stable for (5.1) with respect to all initial conditions in $\operatorname{int}\mathbb{R}^2_+$.

Step 1: Dimensionless rescaling. Introduce $u = x_1/x_1^{**}$, $v = x_2/x_2^{**}$, which maps the coexistence equilibrium to $(1, 1)$. Using the equilibrium identities $\tilde{\alpha}x_2^{**} = \tilde{B}x_1^{**}$ and $\beta x_1^{**} = \tilde{C}x_2^{**} + \gamma(x_2^{**})^2$, the differential equations become

$$\frac{du}{dt} = \tilde{B}(v - u), \tag{5.8a}$$

$$\frac{dv}{dt} = \frac{\beta x_1^{**}}{x_2^{**}}(u - v) - \gamma x_2^{**} v(v - 1). \tag{5.8b}$$

Step 2: Lyapunov function. Define $V : \operatorname{int}\mathbb{R}^2_+ \to \mathbb{R}$ by

$$V(u, v) = (u - 1 - \ln u) + k\,(v - 1 - \ln v), \qquad k := \frac{\tilde{B}\,x_2^{**}}{\beta\,x_1^{**}} > 0. \tag{5.9}$$

The kernel $g(z) = z - 1 - \ln z$ satisfies $g(z) \geq 0$ with $g(1) = 0$ as its unique global minimum. Hence, $V(1, 1) = 0$, $V(u, v) > 0$ for $(u, v) \neq (1, 1)$, and V is radially unbounded.

Step 3: Orbital derivative. Differentiating along (5.8) and grouping the terms, we have

$$\frac{dV}{dt} = \underbrace{\tilde{B}\frac{u - 1}{u}(v - u) + k\frac{\beta x_1^{**}}{x_2^{**}}\frac{v - 1}{v}(u - v)}_{\Sigma_1} \; \underbrace{- \; k\gamma x_2^{**}(v - 1)^2}_{\Sigma_2}. \tag{5.10}$$

By construction, k satisfies $k\beta x_1^{**}/x_2^{**} = \tilde{B}$, so the coefficients in Σ_1 match exactly:

$$\Sigma_1 = \tilde{B}\left[\frac{u - 1}{u}(v - u) + \frac{v - 1}{v}(u - v)\right]. \tag{5.11}$$

The bracket simplifies via elementary algebra:

$$\begin{aligned}\frac{u - 1}{u}(v - u) + \frac{v - 1}{v}(u - v) &= (v - u)\left(\frac{u - 1}{u} - \frac{v - 1}{v}\right) = (v - u)\,\frac{v(u - 1) - u(v - 1)}{uv} \\ &= (v - u)\,\frac{u - v}{uv} = -\frac{(u - v)^2}{uv}.\end{aligned} \tag{5.12}$$

Hence, $\Sigma_1 = -\tilde{B}\,(u - v)^2/(uv)$. Assembling, we have

$$\frac{dV}{dt} = -\tilde{B}\,\frac{(u - v)^2}{uv} - \frac{\tilde{B}\gamma\,(x_2^{**})^2}{\beta x_1^{**}}\,(v - 1)^2. \tag{5.13}$$

All parameters are positive and $u(t), v(t) > 0$ for all $t > 0$. Each term is individually non-positive: the first vanishes iff $u = v$, the second iff $v = 1$. Consequently, $\dot{V} \leq 0$ on $\operatorname{int}\mathbb{R}^2_+$, with $\dot{V} = 0$ iff $(u, v) = (1, 1)$.

Step 4: LaSalle and lifting. Orbits of (5.8) inherit boundedness from the full system via projection and rescaling by fixed positive constants. LaSalle's invariance principle [31, 32] therefore yields $\lim_{t\to\infty}(u(t), v(t)) = (1, 1)$ for all $(u(0), v(0)) \in \operatorname{int}\mathbb{R}^2_+$. Reverting the rescaling gives $\lim_{t\to\infty}(x_1(t), x_2(t)) = (x_1^{**}, x_2^{**})$. Thieme's theorem [28] lifts this to the global asymptotic stability of E^* for the original system (2.1).

Remark 5.4. The weight $k = \tilde{B}x_2^{**}/(\beta x_1^{**}) = \tilde{B}^2/(\tilde{\alpha}\beta)$ (using $x_2^{**}/x_1^{**} = \tilde{B}/\tilde{\alpha}$ from (3.9)) ensures exact cancellation of the $(u - v)$ cross-terms in (5.10), yielding $\dot{V} \leq 0$ with equality only at the equilibrium.

6. Bifurcation analysis

6.1. Transcritical bifurcation at $f = f_{\text{crit}}$

Theorem 6.1 (Transcritical bifurcation)**.** *Assume $f_{\text{crit}} > 0$. Then system* (2.1) *undergoes a transcritical bifurcation at $E_2 = (0, 0, y^*)$ when the fear parameter f passes through f_{crit}.*

Proof. We verify Sotomayor's theorem [32, 33] with f as the bifurcation parameter and $F(X, f) = (F_1, F_2, F_3)^T$ given by (2.1).

Step 0: Zero eigenvalue. From Theorem 4.3(ii), at $f = f_{\text{crit}}$, the Jacobian $J(E_2)$ possesses a simple zero eigenvalue while the other two are $\lambda_2 = -(\tilde{B} + \tilde{C}) < 0$ and $\lambda_3 = -b < 0$. The spectral hypothesis is satisfied.

Step 1: Eigenvectors for $\lambda = 0$. At $f = f_{\text{crit}}$, we have $\mathcal{R}_{\text{fear}} = 1$, which is equivalent to

$$\tilde{\alpha}\beta = \tilde{B}\tilde{C}, \tag{6.1}$$

with $\tilde{\alpha}, \tilde{B}, \tilde{C}$ defined in (3.6). The Jacobian at (E_2, f_{crit}) is

$$J(E_2)\Big|_{f=f_{\text{crit}}} = \begin{bmatrix} -\tilde{B} & \tilde{\alpha} & 0 \\ \beta & -\tilde{C} & 0 \\ 0 & 0 & -b \end{bmatrix}. \tag{6.2}$$

Solving $J\mathbf{v} = \mathbf{0}$ and $\mathbf{w}^T J = \mathbf{0}^T$ with the normalization $v_2 = w_2 = \tilde{B}$ yields

$$\mathbf{v} = \begin{pmatrix} \tilde{\alpha} \\ \tilde{B} \\ 0 \end{pmatrix}, \qquad \mathbf{w} = \begin{pmatrix} \beta \\ \tilde{B} \\ 0 \end{pmatrix}, \qquad \mathbf{w}^T\mathbf{v} = \beta\tilde{\alpha} + \tilde{B}^2 > 0. \tag{6.3}$$

Step 2: Condition (i): $\mathbf{w}^T F_f = 0$. From (2.1), we have

$$\frac{\partial F_1}{\partial f} = -\frac{\alpha y}{(1 + fy)^2}\, x_2, \qquad \frac{\partial F_2}{\partial f} = -\frac{\delta_2 y}{(1 + fy)^2}\, x_2, \qquad \frac{\partial F_3}{\partial f} = 0. \tag{6.4}$$

At $E_2 = (0, 0, y^*)$ the factor $x_2 = 0$ forces every component of $F_f(E_2, f)$ to vanish for *all* $f \geq 0$ (every fear term is multiplied by either x_1 or x_2, both zero at extinction).* Hence, $\mathbf{w}^T F_f(E_2, f_{\text{crit}}) = 0$.

Step 3: Condition (ii): $\mathbf{w}^T[D^2F(\mathbf{v}, \mathbf{v})] \neq 0$. The second Fréchet derivative is $[D^2F(\mathbf{v}, \mathbf{v})]_k = \sum_{i,j=1}^{3} \frac{\partial^2 F_k}{\partial X_i \partial X_j} v_i v_j$. Since $v_3 = 0$ and at E_2, we have $x_1 = x_2 = 0$, the only non-vanishing second derivative contributing to the quadratic form is $\partial^2 F_2/\partial x_2^2 = -2\gamma$. Consequently, we have

$$D^2F(\mathbf{v}, \mathbf{v}) = \begin{pmatrix} 0 \\ -2\gamma\tilde{B}^2 \\ 0 \end{pmatrix}. \tag{6.5}$$

*This structural feature—$F_f(E_2) \equiv \mathbf{0}$ irrespective of f—implies that the bifurcation is driven indirectly: f modifies the effective parameters $\tilde{\alpha}, \tilde{B}, \tilde{C}$ through which the net reproduction number $\mathcal{R}_{\text{fear}}$ changes sign.

Contracting with $\mathbf{w} = (\beta, \tilde{B}, 0)^T$, we have

$$\mathbf{w}^T[D^2F(\mathbf{v},\mathbf{v})] = -2\gamma\tilde{B}^3 \neq 0, \tag{6.6}$$

since $\gamma > 0$ and $\tilde{B} = \beta + \delta_1 + d_1 y^* > 0$.

Step 4: Condition (iii): $\mathbf{w}^T[DF_f\,\mathbf{v}] \neq 0$. From (6.4), differentiating with respect to x_2 and evaluating at E_2 gives the only non-zero entries of the mixed-derivative matrix

$$DF_f(E_2, f_{\text{crit}}) = \begin{bmatrix} 0 & -\dfrac{\alpha y^*}{(1+fy^*)^2} & 0 \\ 0 & -\dfrac{\delta_2 y^*}{(1+fy^*)^2} & 0 \\ 0 & 0 & 0 \end{bmatrix}. \tag{6.7}$$

The $(i, 3)$ entries involve the factor x_2 and also vanish at E_2. Applying to $\mathbf{v} = (\tilde{\alpha}, \tilde{B}, 0)^T$ and contracting with $\mathbf{w}$, we have

$$\mathbf{w}^T[DF_f\,\mathbf{v}] = -\frac{y^*}{(1+fy^*)^2}\,\tilde{B}\,(\alpha\beta + \delta_2\tilde{B}) \neq 0, \tag{6.8}$$

since every factor is strictly positive. The transversality of the eigenvalue crossing is therefore guaranteed.

Step 5: Crossing direction. The eigenvalue crossing speed is [32]

$$\left.\frac{d\lambda_{\text{cross}}}{df}\right|_{f=f_{\text{crit}}} = \frac{\mathbf{w}^T[DF_f\,\mathbf{v}]}{\mathbf{w}^T\mathbf{v}} = -\frac{y^*(1-\Phi)^2\,\tilde{B}\,(\alpha\beta + \delta_2\tilde{B})}{\beta\tilde{\alpha} + \tilde{B}^2} < 0, \tag{6.9}$$

confirming that the crossing eigenvalue decreases through zero as f increases through f_{crit}. All three Sotomayor conditions are therefore satisfied, establishing a transcritical bifurcation at (E_2, f_{crit}).

6.2. Decomposition of the dual fear pathways

The fear threshold admits the explicit representation

$$f_{\text{crit}} = \frac{\dfrac{\alpha\beta}{\tilde{B}} - \delta_2 - d_2 y^*}{y^*(2\delta_2 + d_2 y^*)}, \qquad \tilde{B} = \beta + \delta_1 + d_1 y^*. \tag{6.10}$$

Fear operates through two pathways: The reproductive pathway $\alpha \mapsto \alpha/(1 + fy)$ restricts the recruitment of new individuals, and the mortality pathway $\delta_2 \mapsto \delta_2(1 + fy/(1 + fy))$ widens adult attrition. We disentangle their interaction analytically.

Birth-only variant. Let $f_{\text{crit}}^{(b)}$ be the threshold when fear acts only on birth (i.e., $\tilde{C} = \delta_2 + d_2 y^*$). The same derivation yields

$$f_{\text{crit}}^{(b)} = \frac{\dfrac{\alpha\beta}{\tilde{B}} - \delta_2 - d_2 y^*}{y^*(\delta_2 + d_2 y^*)}. \tag{6.11}$$

Comparing the denominators, we have

$$f_{\text{crit}} < f_{\text{crit}}^{(b)}, \tag{6.12}$$

so that adding mortality fear strictly lowers the extinction threshold compared with birth fear alone.

Death-only variant. When fear affects only mortality ($\tilde{\alpha} = \alpha$ unchanged), the effective adult loss rate $\tilde{C}(f) = \delta_2(1 + fy^*/(1 + fy^*)) + d_2 y^*$ saturates to $\tilde{C}_{\max} = 2\delta_2 + d_2 y^*$ as $f \to \infty$. Death fear alone extinguishes the population if and only if $\alpha\beta/\tilde{B} \le \tilde{C}_{\max}$; otherwise, the mortality pathway saturates before closing the net growth gap, and no finite $f_{\text{crit}}^{(d)}$ exists. This asymmetry—the reproductive pathway being the indispensable extinction driver while the mortality pathway has a structurally limited capacity—is absent from formulations with unbounded or symmetric fear effects. Numerical confirmation appears in Section 7.4.

7. Numerical simulations

All numerical integrations are performed using the classical fourth-order Runge–Kutta method (RK4) with a fixed step size $\Delta t = 0.01$ over the interval $t \in [0, 200]$, which is sufficiently long for all solutions to approach their asymptotic limits. Computations were carried out in MATLAB R2023a (MathWorks, Natick, MA, USA) on a standard desktop machine. Numerical non-negativity was monitored at every integration step; no negative values were observed in any of the reported simulations. The code is available from the corresponding author upon reasonable request. The baseline parameter set, used throughout this section unless stated otherwise, is

$$\alpha = 2.0,\ \ \beta = 0.8,\ \ \delta_1 = 0.3,\ \ \delta_2 = 0.4,\ \ \gamma = 0.05,\ \ d_1 = 0.02,\ \ d_2 = 0.03,\ \ b = 1.0,\ \ a = 0.1, \tag{7.1}$$

which yields $y^* = 10$, $\mathcal{N}_0 \approx 3.64 > 1$, and $f_{\text{crit}} \approx 0.0483$. Unless otherwise stated, the initial conditions for phase portraits and time series are $(x_1(0), x_2(0), y(0)) = (2, 4, 5)$, $(8, 2, 8)$, and $(5, 8, 12)$, representing three ecologically distinct starting configurations (juvenile-dominated, adult-dominated, and balanced, respectively).

7.1. Model validation: Stability and bifurcation

Figures 1 and 2 validate the core theoretical predictions. Figure 1 presents the transcritical bifurcation diagram: The stable E^* branch (solid blue) exists for $f < f_{\text{crit}}$, the infeasible branch (dashed blue) for $f > f_{\text{crit}}$, and the E_2 branch (red) exchanges stability at the bifurcation point $f = f_{\text{crit}} \approx 0.0483$.

Figure 2 tracks the eigenvalues of $J(E_2)$ as f varies. One eigenvalue crosses zero from positive to negative at $f = f_{\text{crit}}$, confirming the stability exchange. The eigenvalue $\lambda_3 = -b = -1$ remains constant.

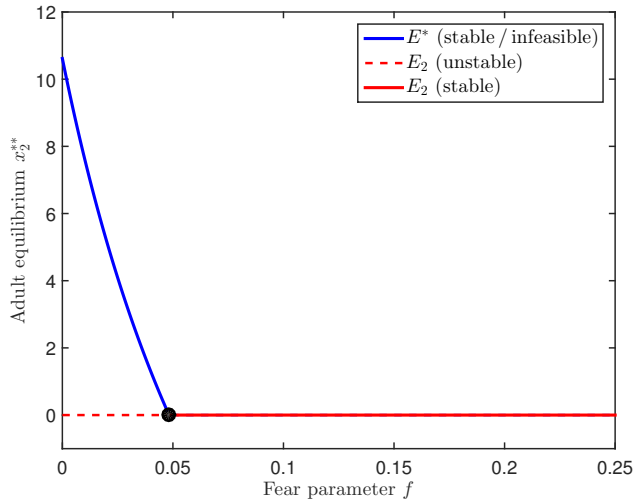

Figure 1. Transcritical bifurcation diagram: x_2^{**} vs. f. Solid: Stable; dashed: Unstable/infeasible. $f_{\text{crit}} \approx 0.0483$. Baseline parameter values are given in (7.1).

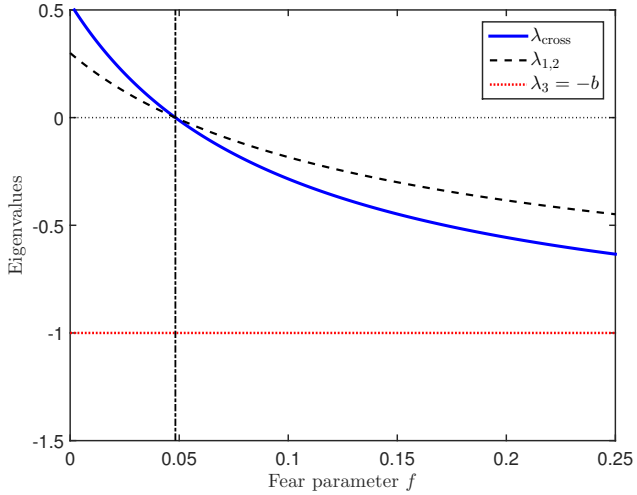

Figure 2. Eigenvalues of $J(E_2)$ vs. f. λ_{cross} (solid) crosses zero at $f_{\text{crit}} \approx 0.0483$; remaining $\lambda_{1,2}, \lambda_3$ stay negative. Baseline parameter values are given in (7.1).

Figures 3–6 illustrate the two dynamic regimes. In the coexistence regime ($f = 0.02 < f_{\text{crit}}$, Figure 3), all trajectories converge monotonically to $E^* \approx (6.64, 5.18, 10)$ from diverse initial conditions. In the extinction regime ($f = 0.10 > f_{\text{crit}}$, Figure 4), Species 1 is deterministically driven to extinction. The convergence is monotonic in both cases, consistent with the proved absence of Hopf bifurcation (Remark 4.6).

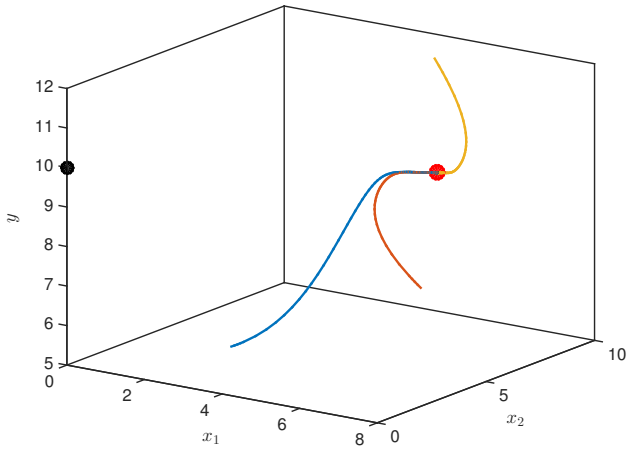

Figure 3. Phase portrait: Coexistence ($f = 0.02 < f_{\text{crit}}$). Three trajectories converge to E^* (red dot); black dot: E_2. The baseline parameter set (7.1) was used, and $y(0) = 5$.

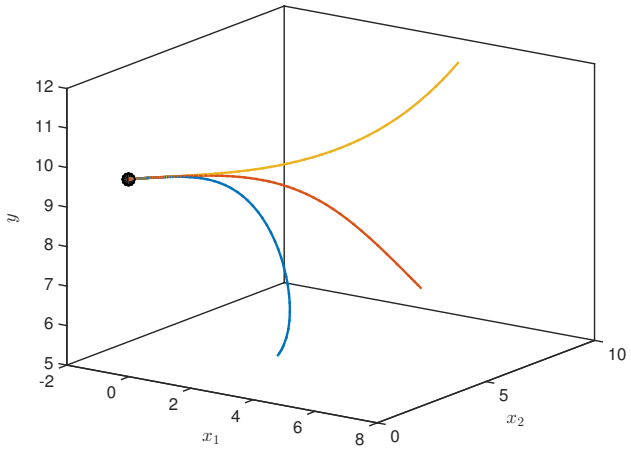

Figure 4. Phase portrait: Extinction ($f = 0.10 > f_{\text{crit}}$). Three trajectories converge to E_2 (black dot). The baseline parameter set (7.1) was used, and $y(0) = 5$.

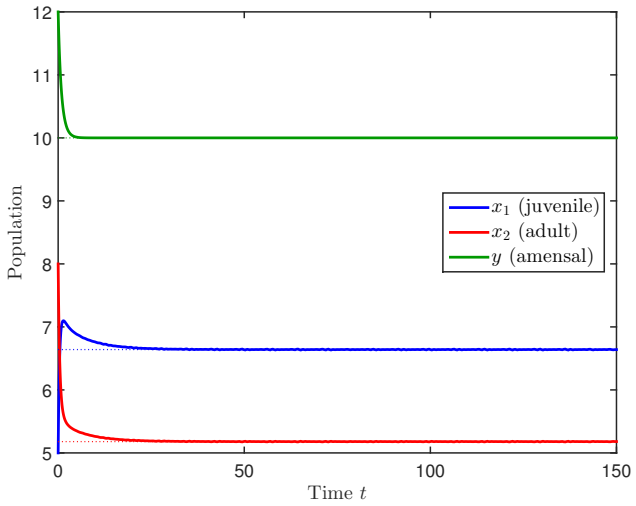

Figure 5. Time series: Coexistence ($f = 0.02$). Blue: x_1, red: x_2, green: y. Initial: $(x_1(0), x_2(0), y(0)) = (5, 8, 12)$. The baseline parameter set (7.1) was used.

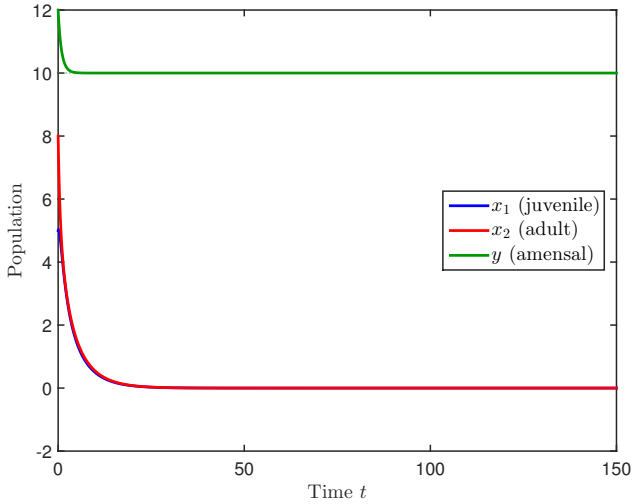

Figure 6. Time series: Extinction ($f = 0.10$). Blue: x_1, red: x_2, green: y. Initial: $(5, 8, 12)$. The baseline parameter set (7.1) was used.

7.2. Lyapunov function verification

Figures 7 and 8 demonstrate the monotonic decay of the constructed Lyapunov functions, providing numerical confirmation of the global stability proofs. Both $V(t)$ (Theorem 5.3) and $W(t)$ (Theorem 5.2) decrease strictly to zero, confirming that the Lyapunov functions correctly certify the global convergence. In the coexistence regime ($f = 0.02 < f_{\text{crit}}$), the logarithmic Lyapunov function $V(t)$ drops sharply at first, then gradually levels off toward zero, since $\dot{V}$ is strictly negative away from equilibrium. At the bifurcation point ($f = f_{\text{crit}} \approx 0.0483$), the linear Lyapunov function $W(t)$ also decays to zero. This is less obvious, because the Jacobian at E_2 is non-hyperbolic (Theorem 5.2), yet the decay remains monotonic, governed simply by $\dot{W} = -\tilde{B}\gamma x_2^2 \leq 0$.

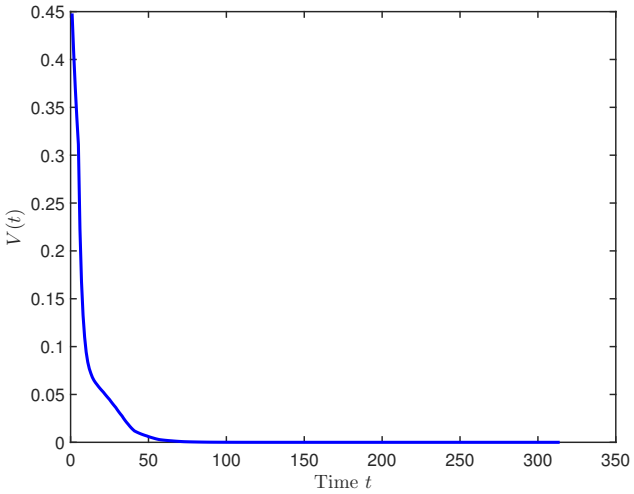

Figure 7. Lyapunov function $V(t)$ (Theorem 5.3): Coexistence ($f = 0.02$). Initial: $(8, 2)$. The baseline parameter set (7.1) was used.

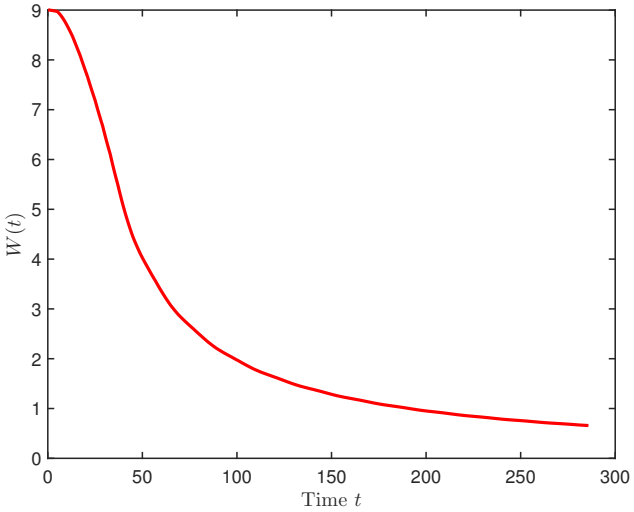

Figure 8. Lyapunov function $W(t)$ (Theorem 5.2): At the bifurcation point $f = f_{\text{crit}} \approx 0.0483$. Initial: $(8, 2)$. The baseline parameter set (7.1) was used.

7.3. Two-parameter stability analysis

Figure 9 maps the stability regions in the $(\mathcal{N}_0, f)$ parameter plane, providing a global view of the system's dynamic possibilities. The green region corresponds to coexistence (E^* globally stable), while the red region corresponds to the extinction of Species 1. The boundary is given by $f = f_{\text{crit}}(\mathcal{N}_0)$. For $\mathcal{N}_0 < 1$, extinction is unconditional regardless of f, consistent with the fact that Species 1 cannot persist even in the absence of the amensal species. Within the coexistence region ($\mathcal{N}_0 > 1$, $f < f_{\text{crit}}$), the threshold f_{crit} decreases monotonically with $\mathcal{N}_0$, indicating that populations with a higher baseline reproductive capacity tolerate greater fear intensity before being driven to extinction.

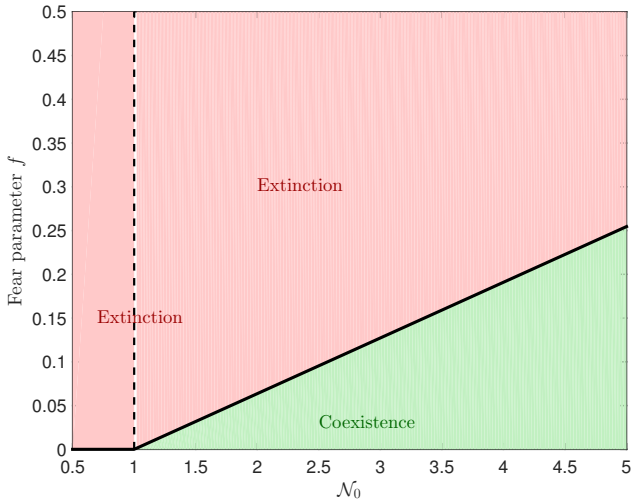

Figure 9. Stability regions in $(\mathcal{N}_0, f)$ plane. Green: Coexistence; red: Extinction. Boundary: $f = f_{\text{crit}}(\mathcal{N}_0)$. The value of α varied; other parameters were taken from (7.1).

7.4. Model-variant comparison: Quantifying dual-pathway interaction

To disentangle the contributions of the two fear pathways and to quantify their interaction, we conduct a numerical model-variant comparison. Three variants of the model are simulated: The original model (both pathways active), the birth-only variant (fear acts solely on $\alpha/(1 + fy)$ with δ_2 being unchanged), and the death-only variant (fear acts solely on $\delta_2(1 + fy/(1 + fy))$ with α being unchanged). For each variant, we compute the adult equilibrium density x_2^{**} as a function of the fear parameter f and determine the corresponding critical threshold.

With the baseline parameters, we obtain $f_{\text{crit}} \approx 0.0483$ (both pathways), $f_{\text{crit}}^{(b)} \approx 0.0758$ (birth fear only). For the death-only variant, $\alpha\beta/\tilde{B} = 1.231$ and $\tilde{C}_{\max} = 1.1 < 1.231$, so pure death fear cannot drive extinction with this parameter set: The amplifying effect saturates at $2\delta_2 = 0.8$, which is insufficient to close the net growth gap of 0.531 created by direct harm. This highlights the essential role of the reproductive pathway as the dominant extinction driver, with the mortality pathway acting as an amplifying factor.

The results, presented in Figure 10, reveal three important findings. First, the critical fear threshold under the combined pathways ($f_{\text{crit}} \approx 0.0483$) is substantially lower than under the birth-only pathway ($f_{\text{crit}}^{(b)} \approx 0.0758$). This confirms the analytical prediction (6.12) and demonstrates that the two pathways produce a threshold-lowering interaction. Second, with the baseline parameters, the death-only pathway cannot independently drive the population to extinction because the maximum mortality amplification (approaching $2\delta_2 = 0.8$) is insufficient to overcome the net growth in the absence of reproductive suppression. Third, the slope of the combined curve is steeper than that of the birth-only curve, indicating that the amplifying effect intensifies as f increases.

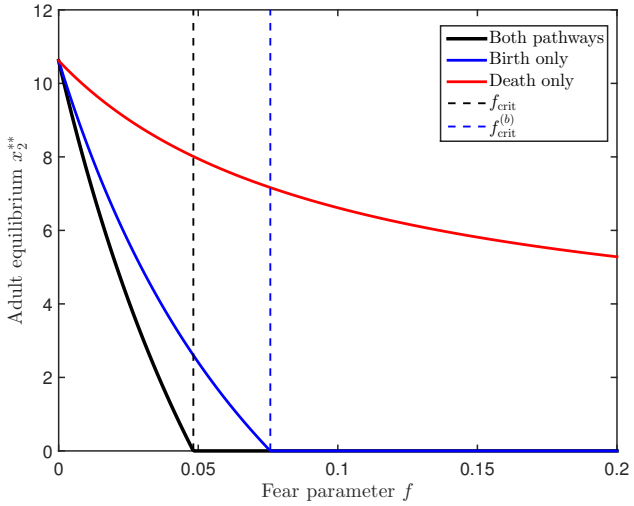

Figure 10. Model-variant comparison: x_2^{**} vs. f. Black: Both pathways ($f_{\text{crit}} \approx 0.0483$); blue: Birth only ($f_{\text{crit}}^{(b)} \approx 0.0758$); red: Death only (no finite threshold). Baseline parameters were taken from (7.1).

7.5. Parameter sensitivity of the extinction threshold

As shown in Figure 11, f_{crit} decreases with increasing δ_2, reflecting the intuitive fact that populations with higher baseline adult mortality are more vulnerable to fear-induced extinction. Figure 12 demonstrates that f_{crit} also decreases with an increasing y^*, indicating that higher amensal densities make the inhibited species less tolerant of fear. Both trends are observed under the baseline parameter set (7.1); the signs of the partial derivatives $\partial f_{\text{crit}}/\partial \delta_2$ and $\partial f_{\text{crit}}/\partial y^*$ may depend on the parameter regime and are not claimed as universal monotonicities.

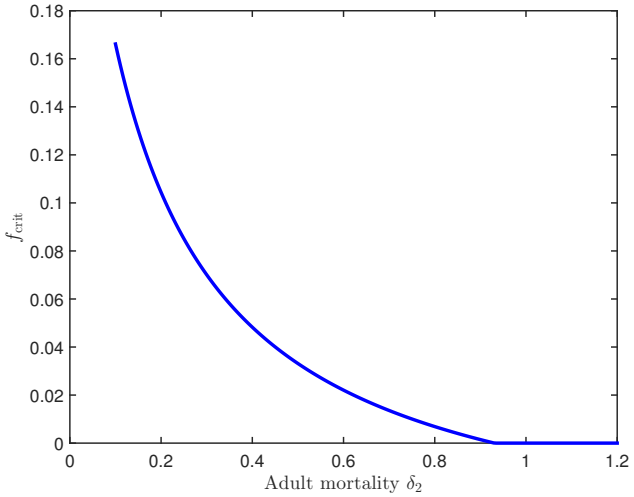

Figure 11. f_{crit} vs. adult mortality δ_2. Other parameters were taken from (7.1).

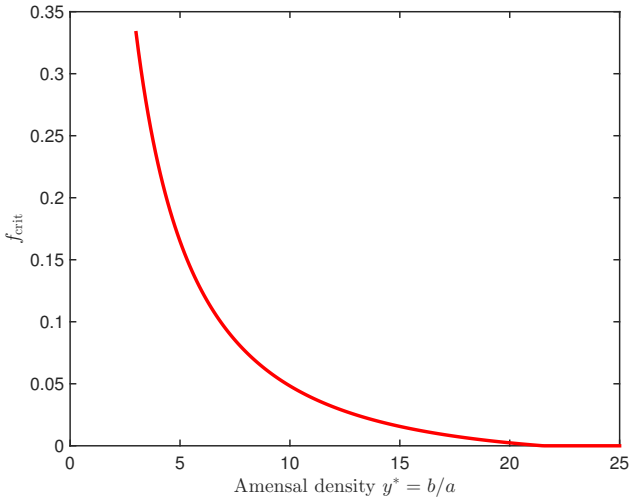

Figure 12. f_{crit} vs. amensal density $y^* = b/a$. Here b varied, $a = 0.1$ fixed; other parameters were taken from (7.1).

7.6. Comparison with Chong et al. (2024): Isolated pathway effects

To facilitate a direct comparison with the sensitivity analysis of Chong et al. [10] (their Figures 4 and 5), we examine the effect of each fear pathway in isolation through separate model variants. Figures 13 and 14 display x_2^{**} as a function of f when only birth fear is active (Figure 13) and when only death fear is active (Figure 14). In the birth-only case, x_2^{**} decreases monotonically to zero as f increases past $f_{\text{crit}}^{(b)} \approx 0.0758$, confirming that reproductive suppression alone can drive extinction. In the death-only case, x_2^{**} decreases but stabilizes at a positive asymptote, reflecting the bounded nature of the mortality amplification. This contrast vividly illustrates why the combined action of both pathways yields a threshold lower than the birth-only threshold, while the death-only pathway may lack a finite threshold altogether.

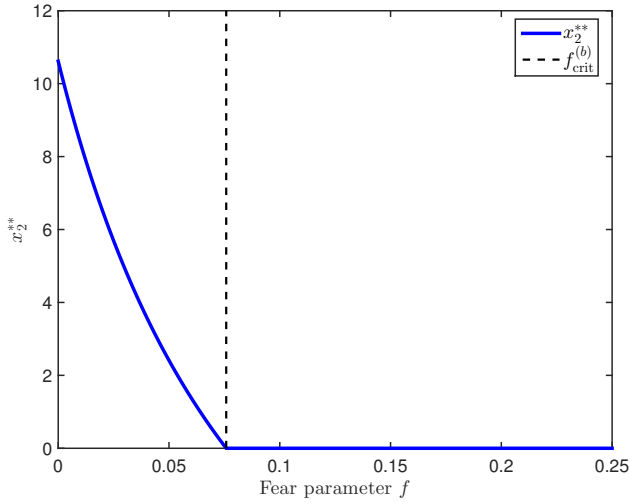

Figure 13. Birth fear only: x_2^{**} vs. f. $f_{\text{crit}}^{(b)} \approx 0.0758$ (dashed). Baseline parameters were taken from (7.1).

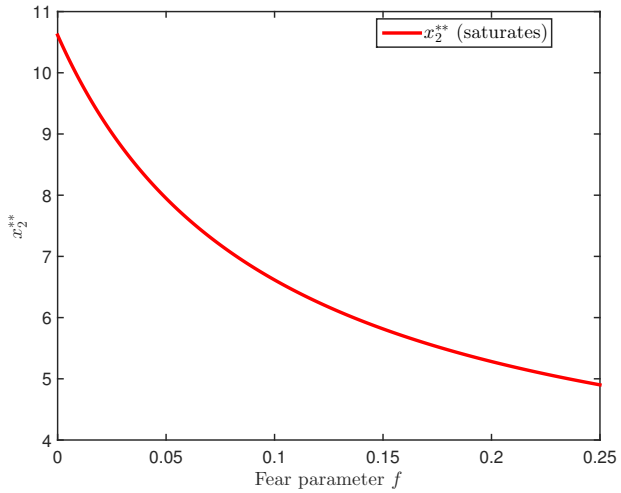

Figure 14. Death fear only: x_2^{**} vs. f. Saturates at positive asymptote (no finite threshold). Baseline parameters were taken from (7.1).

8. Discussion

8.1. Comparison with related models

The present model integrates two previously separate frameworks: Lei [27] (stage-structured amensalism without fear) and Chong et al. [10] (unstructured amensalism with fear). Table 2 provides a structured comparison.

Table 2. Comparison among related amensalism models.

Aspect	Lei (2018)	Chong et al. (2024)	Present model
Stage structure	Yes (Species 1)	No	Yes (Species 1)
Fear effect	No	Yes	Yes
Fear parameters	—	2 (k_1, k_2)	1 (f)
Death-fear form	—	Linear, unbounded	Saturated, bounded
Death upper bound	—	None	$2\delta_2$
Bifurcation	Not analyzed	Not analyzed	Transcritical
Hopf bifurcation	Not addressed	Not addressed	Proved structurally absent
Model-variant comparison	—	Separate Figures 4 and 5	Unified (Figure 10)
Global stability	Proved	Proved	Proved

The model differs from its predecessors in three respects. First, the saturated death-fear formulation $\delta_2(1 + fy/(1 + fy))$ approaches the finite limit $2\delta_2$, providing a bounded alternative to the linear formulation in Chong et al. [10]. Second, Hopf bifurcation is structurally excluded (Remark 4.6): The block upper-triangular Jacobian confines the search for purely imaginary eigenvalues to the 2×2 subsystem, whose strictly negative trace then precludes them. This structural property also holds for the autonomous Chong et al. model. Third, the model-variant comparison

(Figure 10) shows that the combined threshold $f_{\text{crit}} \approx 0.0483$ is strictly lower than the birth-only threshold $f_{\text{crit}}^{(b)} \approx 0.0758$, indicating a threshold-lowering interaction between the two fear pathways.

8.2. Biological implications

The transcritical bifurcation has implications for conservation biology. Fear-inducing species can drive vulnerable native populations to extinction even without causing physical harm, if fear intensity exceeds the critical threshold. This is relevant for introduced predators [34], ecotourism-induced chronic stress [35], and allelopathic invasions. The parameter sensitivity analysis (Figures 11 and 12) further reveals that populations with high baseline adult mortality (δ_2) or those exposed to high amensal densities (y^*) are disproportionately vulnerable to fear-induced extinction.

The model-variant comparison suggests a possible management implication. The finding that the reproductive pathway is the dominant extinction driver under our parameterization suggests that management interventions aimed at protecting reproductive output (e.g., creating birthing refuges, reducing disturbance during breeding seasons) may yield greater conservation benefits than interventions targeting adult survival alone. However, because the mortality pathway amplifies the effect of the reproductive pathway (as quantified by $f_{\text{crit}} < f_{\text{crit}}^{(b)}$), combined interventions addressing both pathways simultaneously will be most effective.

8.3. Limitations and scope

Several limitations of the present study should be acknowledged. First, we restricted fear effects to adult mortality and reproduction only, leaving juvenile maturation (β) and juvenile mortality (δ_1) unmodified. This is a deliberate modeling simplification, ecologically motivated by three considerations (Section 2.1): Adults are the primary perceivers of threat cues, the empirical evidence of Zanette et al. [15] points predominantly to reproductive rather than juvenile-survival effects, and parsimony favours confining the new parameter f to the two most strongly supported channels. However, in systems where juveniles are directly exposed to amensal disturbances—for example, ground-nesting bird chicks trampled by large herbivores—fear-induced juvenile mortality or delayed maturation may be ecologically significant. Extending the model to include fear-modulated β or δ_1 would broaden applicability and could reveal whether the dual-pathway interaction identified here extends to juvenile-stage pathways as well. Second, the use of a single fear parameter f governing both pathways assumes a perfect correlation between reproductive and mortality fear sensitivities. In reality, these may be decoupled, and a two-parameter extension permitting independent sensitivities could reveal richer dynamic structures. Third, the saturation level $2\delta_2$ of the mortality amplification is a direct consequence of the chosen Holling-Type II response form rather than an empirically calibrated physiological limit; alternative saturating functions would yield different ceilings while preserving the same qualitative threshold structure.

Finally, we address two degenerate parameter regimes that are excluded from the main analysis but are structurally important for completeness. If $\mathcal{N}_0 \leq 1$, Species 1 cannot persist even in the absence of the amensal species ($y = 0$); in this case, E_1 does not exist, and E_2 is the only feasible equilibrium for all $f \geq 0$, so extinction is unconditional and fear is irrelevant. If $\mathcal{N}_0 > 1$ but $f_{\text{crit}} \leq 0$ (i.e., the direct amensal harm alone is sufficiently severe that $\alpha\beta/\tilde{B} \leq \delta_2 + d_2 y^*$), then Species 1 is driven to extinction even at $f = 0$: The coexistence branch E^* lies entirely in the unphysical region $f < f_{\text{crit}} \leq 0$,

and fear merely accelerates an extinction that is already deterministic. Both regimes are covered by Theorem 3.3—the transcritical bifurcation formally occurs at a non-positive value of the bifurcation parameter, so the coexistence branch is inaccessible for any physically admissible $f \geq 0$—and they serve as useful reminders that fear is an aggravating factor superimposed on an already existing amensal pressure, not necessarily the primary cause of extinction.

Future research directions. The present work establishes a deterministic baseline; several extensions appear both ecologically warranted and mathematically tractable.

(i) **Temporal delays and transient dynamics.** Introducing a maturation time delay τ (so that $\beta x_1(t-\tau)$ replaces $\beta x_1(t)$ in the adult equation) would bring the model closer to the physiological reality of stage-structured populations [24]. Delays could destabilize the coexistence equilibrium through Hopf bifurcation, a phenomenon structurally absent in the ODE case, potentially generating fear-induced oscillations of ecological relevance.

(ii) **Stochastic formulations.** Recasting the model as a stochastic differential system would permit the estimation of extinction probabilities and mean first-passage times in the vicinity of the deterministic threshold f_{crit}, yielding risk metrics that are directly applicable to conservation triage.

(iii) **Spatial structure.** Embedding the model in a spatial domain via the diffusion terms $D_1\Delta x_1$, $D_2\Delta x_2$ would allow the study of fear-driven spatial patterns, critical patch sizes for persistence, and travelling wave solutions connecting the extinction and coexistence states.

(iv) **Multi-species and community-level extensions.** Extending the framework to food webs where the amensal species occupies an intermediate trophic level, or where multiple species are simultaneously affected by fear, would test whether the dual-pathway amplifying mechanism identified here generalizes to more complex interaction networks.

(v) **Empirical calibration.** The single fear parameter f encapsulates both reproductive suppression and mortality amplification. Controlled mesocosm experiments (e.g., manipulating perceived amensal density while measuring both fecundity and adult survival) could estimate f for specific study systems, enabling a quantitative comparison between theoretical thresholds and field observations.

9. Conclusions

This paper introduces a bounded fear-mortality mechanism into Lei's [27] stage-structured amensalism framework, extending the model beyond the unstructured formulation of Chong et al. [10]. The analysis yields a dynamic classification governed by a single critical threshold f_{crit}, with three central findings.

(i) **Bifurcation structure.** The system exhibits a transcritical bifurcation at $f = f_{\text{crit}}$, verified through Sotomayor's theorem. The crossing direction $d\lambda_{\text{cross}}/df|_{f=f_{\text{crit}}} < 0$ confirms the stability exchange: E_2 is unstable for $f < f_{\text{crit}}$ and stable for $f > f_{\text{crit}}$, while the coexistence equilibrium E^* exists and is stable exactly when $f < f_{\text{crit}}$. This defines a precise boundary between coexistence ($f < f_{\text{crit}}$) and extinction ($f \geq f_{\text{crit}}$), with the extinction equilibrium globally asymptotically stable at the

bifurcation point itself. As a structural corollary of the block upper-triangular Jacobian—which follows from the decoupled amensal dynamics—Hopf bifurcation is precluded at every admissible equilibrium, simplifying the dynamic repertoire to a pure transcritical exchange of stability.

(ii) **Global stability.** Global stability is established in both regimes using complementary Lyapunov constructions: A Volterra-type logarithmic function for the coexistence equilibrium, and a linear function for the extinction equilibrium whose analysis extends continuously through the bifurcation point.

(iii) **Dual-pathway amplifying interaction.** The interaction between reproductive suppression and mortality amplification is quantified analytically and confirmed numerically: The combined threshold is strictly lower than the birth-only threshold. The saturated mortality response $\delta_2(1 + fy/(1 + fy))$, bounded by $2\delta_2$, provides a conservative, ecologically motivated alternative to the unbounded linear formulation in Chong et al. while maintaining analytical tractability.

The model adds one parameter to Lei's [27] framework and may serve as a baseline for further theoretical and empirical investigations of fear effects in structured ecological communities.

Use of AI tools declaration

The authors declare they have not used artificial intelligence (AI) tools in the creation of this article.

Acknowledgments

This research was funded by the Social Science Project of Anhui Provincial Department of Education (2025AHGXSK30179), Anhui Provincial Research Center for Eco-agriculture of Chinese Medicinal Herbs Research Platform Project and the Natural Science Foundation of Fujian Province (2024J01273).

Conflict of interest

The authors declare there are no conflicts of interest.

References

1. R. H. Whittaker, *Communities and Ecosystems*, Macmillan, New York, 1975.
2. E. L. Rice, *Allelopathy*, Academic Press, Orlando, 1984.
3. J. F. Zhang, Bifurcated periodic solutions in an amensalism system with strong generic delay kernel, *Math. Methods Appl. Sci.*, **36** (2013), 113–124. https://doi.org/10.1002/mma.2575
4. X. Y. Guan, F. D. Chen, Dynamical analysis of a two species amensalism model with Beddington–DeAngelis functional response and Allee effect on the second species, *Nonlinear Anal. Real World Appl.*, **48** (2019), 71–93. https://doi.org/10.1016/j.nonrwa.2019.01.002
5. Q. Zhou, F. Chen, Dynamical analysis of a discrete amensalism system with the Beddington–DeAngelis functional response and Allee effect for the unaffected species, *Qual. Theory Dyn. Syst.*, **22** (2023), 16. https://doi.org/10.1007/s12346-022-00716-5

6. D. Luo, Q. Wang, Global dynamics of a Beddington–DeAngelis amensalism system with weak Allee effect on the first species, *Appl. Math. Comput.*, **408** (2021), 126368. https://doi.org/10.1016/j.amc.2021.126368
7. Q. Li, F. Chen, L. Chen, Z. Li, Dynamical analysis of a discrete amensalism system with Michaelis–Menten type harvesting for the second species, *Qual. Theory Dyn. Syst.*, **23** (2024), 279. https://doi.org/10.1007/s12346-024-01142-5
8. A. Alhadi, R. K. Naji, The role of amensalism and parasitism on the dynamics of three species ecological system, *Results Control Optim.*, **19** (2025), 100571. https://doi.org/10.1016/j.rico.2025.100571
9. X. Xi, J. N. Griffin, S. Sun, Grasshoppers amensalistically suppress caterpillar performance and enhance plant biomass in an alpine meadow, *Oikos*, **122** (2013), 1049–1057. https://doi.org/10.1111/j.1600-0706.2012.00126.x
10. Y. Chong, Y. Hou, S. Chen, F. Chen, The influence of fear effect to the dynamic behaviors of Lotka–Volterra amensalism model, *Eng. Lett.*, **32** (2024), 1233–1242.
11. Q. Zhu, F. Chen, Z. Li, L. Chen, Global dynamics of two-species amensalism model with Beddington–DeAngelis functional response and fear effect, *Int. J. Bifurcation Chaos*, **34** (2024), 2450075. https://doi.org/10.1142/S0218127424500755
12. Q. Li, A. J. Kashyap, Q. Zhu, F. Chen, Dynamical behaviours of discrete amensalism system with fear effects on first species, *Math. Biosci. Eng.*, **21** (2024), 832–860. https://doi.org/10.3934/mbe.2024035
13. S. J. Aldosari, R. Ahmed, Dynamics and bifurcation analysis of a discrete amensalism model with fear effect, *Int. J. Dyn. Control*, **14** (2026), 99. https://doi.org/10.1007/s40435-026-02040-1
14. Q. Li, F. Chen, L. Chen, Z. Li, Dynamical analysis of a discrete amensalism system with the Beddington–DeAngelis functional response and fear effect, *J. Appl. Anal. Comput.*, **15** (2025), 2089–2123. https://doi.org/10.11948/20240399
15. L. Y. Zanette, A. F. White, M. C. Allen, M. Clinchy, Perceived predation risk reduces the number of offspring songbirds produce per year, *Science*, **334** (2011), 1398–1401. https://doi.org/10.1126/science.1210908
16. M. J. Sheriff, C. J. Krebs, R. Boonstra, The sensitive hare: sublethal effects of predator stress on reproduction in snowshoe hares, *J. Anim. Ecol.*, **78** (2009), 1249–1258. https://doi.org/10.1111/j.1365-2656.2009.01552.x
17. S. Creel, D. Christianson, S. Liley, J. A. Winnie, Predation risk affects reproductive physiology and demography of elk, *Science*, **315** (2007), 960. https://doi.org/10.1126/science.1135918
18. R. M. Sapolsky, L. M. Romero, A. U. Munck, How do glucocorticoids influence stress responses? integrating permissive, suppressive, stimulatory, and preparative actions, *Endocr. Rev.*, **21** (2000), 55–89. https://doi.org/10.1210/edrv.21.1.0389
19. J. S. Brown, J. W. Laundré, M. Gurung, The ecology of fear: optimal foraging, game theory, and trophic interactions, *J. Mammal.*, **80** (1999), 385–399. https://doi.org/10.2307/1383287
20. M. J. Sheriff, O. P. Love, Determining the adaptive potential of maternal stress, *Ecol. Lett.*, **16** (2013), 271–280. https://doi.org/10.1111/ele.12042

21. X. Wang, L. Zanette, X. Zou, Modelling the fear effect in predator-prey interactions, *J. Math. Biol.*, **73** (2016), 1179–1204. https://doi.org/10.1007/s00285-016-0989-1
22. S. K. Sasmal, Y. Takeuchi, Dynamics of a predator-prey system with fear and group defense, *J. Math. Anal. Appl.*, **481** (2020), 123471. https://doi.org/10.1016/j.jmaa.2019.123471
23. S. Mondal, A. Maiti, G. P. Samanta, Effects of fear and additional food in a delayed predator-prey model, *Biophys. Rev. Lett.*, **13** (2018), 157–177. https://doi.org/10.1142/S1793048018500091
24. W. G. Aiello, H. I. Freedman, A time-delay model of single-species growth with stage structure, *Math. Biosci.*, **101** (1990), 139–153. https://doi.org/10.1016/0025-5564(90)90019-U
25. R. Xu, Z. Ma, Stability and Hopf bifurcation in a predator-prey model with stage structure for the predator, *Nonlinear Anal. Real World Appl.*, **9** (2008), 1444–1460. https://doi.org/10.1016/j.nonrwa.2007.03.015
26. S. Khajanchi, Modeling the dynamics of stage-structure predator-prey system with Monod–Haldane type response function, *Appl. Math. Comput.*, **302** (2017), 122–143. https://doi.org/10.1016/j.amc.2017.01.019
27. C. Lei, Dynamic behaviors of a stage structure amensalism system with a cover for the first species, *Adv. Differ. Equations*, **2018** (2018), 272. https://doi.org/10.1186/s13662-018-1729-1
28. H. R. Thieme, Convergence results and a Poincaré–Bendixson trichotomy for asymptotically autonomous differential equations, *J. Math. Biol.*, **30** (1992), 755–763. https://doi.org/10.1007/BF00173267
29. H. L. Smith, *Monotone Dynamical Systems*, American Mathematical Society, Providence, 1995.
30. P. Hartman, *Ordinary Differential Equations*, SIAM, Philadelphia, 2002. https://doi.org/10.1137/1.9780898719222
31. S. Wiggins, *Introduction to Applied Nonlinear Dynamical Systems and Chaos*, Springer, New York, 2003.
32. Y. A. Kuznetsov, *Elements of Applied Bifurcation Theory*, Springer, New York, 2004. https://doi.org/10.1007/978-1-4757-3978-7
33. J. Sotomayor, Generic bifurcations of dynamical systems, in *Dynamical Systems*, Academic Press, New York, (1973), 561–582. https://doi.org/10.1016/B978-0-12-550350-1.50047-3
34. T. S. Doherty, A. S. Glen, D. G. Nimmo, E. G. Ritchie, C. R. Dickman, Invasive predators and global biodiversity loss, *Proc. Natl. Acad. Sci. U.S.A.*, **113** (2016), 11261–11265. https://doi.org/10.1073/pnas.1602480113
35. S. Ciuti, J. M. Northrup, T. B. Muhly, S. Simi, M. Musiani, J. A. Pitt, et al., Effects of humans on behaviour of wildlife exceed those of natural predators in a landscape of fear, *PLoS One*, **7** (2012), e50611. https://doi.org/10.1371/journal.pone.0050611